Journal of Magnetism and Magnetic Materials 454 (2018) 131–138

Contents lists available at ScienceDirect

Journal of Magnetism and Magnetic Materials

journal homepage: www.elsevier.com/locate/jmmm

Research articles

Magnetic oscillations in silicene

F. Escudero [a,b,*], J.S. Ardenghi [a,b], P. Jasen [a,b]

[a] Departamento de Física, Universidad Nacional del Sur, Av. Alem 1253, B8000CPB Bahía Blanca, Argentina
[b] Instituto de Física del Sur (IFISUR, UNS-CONICET), Av. Alem 1253, B8000CPB Bahía Blanca, Argentina

ARTICLE INFO

Article history:
Received 5 May 2017
Received in revised form 3 December 2017
Accepted 22 January 2018

ABSTRACT

In this work the magnetic oscillations (MO) in pristine silicene at $T = 0$ K are studied. Considering a constant electron density we obtain analytical expressions for the ground state internal energy and magnetization, under a perpendicular electric and magnetic field, taking in consideration the Zeeman effect. It is found that the MO are sawtooth-like, depending on the change in the last occupied energy level. This leads us to a classification of the MO peaks in terms of the Landau level (LL), valley or spin changes. Using this classification we analyze the MO for different values of the electric field E_z. When $E_z = 0$, the energy levels have a valley degeneracy and the MO peaks occur only whenever the last energy level changes its LL and/or spin. When $E_z \neq 0$, the valley degeneracy is broken and new MO peaks appear, associated with the valley change in the last energy level. By analyzing the MO peaks amplitude it is possible to extract information about the Fermi velocity and the spin-orbit interaction strength. Finally we analyze the MO frequencies, which can also be associated with the change of LL, valley or spin in the last energy level.

1. Introduction

In the past few years silicene has been gaining considerable interest in the scientific community [1–3]. Like graphene, silicene has a 2D hexagonal structure with silicon atoms at each lattice site, with two interpenetrating sublattices *A* and *B*. The reciprocal space is also a hexagonal lattice in the momentum space, which in turn defines the Brillouin zone. Silicene is best described with a tight binding (TB) model, which leads to an effective Dirac-like Hamiltonian in the low energy approximation, with the sublattices *A* and *B* acting as a pseudospin degree of freedom [4–6]. Nevertheless, silicene distinguish itself from graphene by two important features. One is the large spin-orbit interaction (SOI), about 3.9 meV [7] (compared to 10^{-3} meV in graphene [8]), which makes silicene a topological insulator. Moreover, this strong SOI would make possible the observation of the quantum spin Hall effect [9–12]. The other characteristic is that the lattice structure in silicene is not planar but buckled, with a layer separation between the two sublattices [2]. Thus by introducing a potential difference between the two sublattices one can tune the bandgap [13–16]. These features imply than in silicene at low energies the electrons behave as massive Dirac fermions [17], moving with a Fermi velocity of about 5.5×10^5 m/s [4,18].

When a magnetic field is applied to silicene, the discrete Landau levels (LL) are obtained. As in graphene, due to the relativistic-like dispersion relation these levels are not equidistant [19]. Moreover, the Landau energy in silicene is smaller than in graphene, due to the bigger Fermi velocity in the latter. The LL create an oscillating behavior in the thermodynamics potentials. For instance, the magnetization oscillates as a function of the inverse magnetic field, the so called de Haas van Alphen (dHvA) effect [20]. The different frequencies involved in the oscillations are related to the closed orbits that electrons perform on the Fermi surface. This effect is purely quantum mechanical and is an useful tool to map the Fermi surface [21]. In graphene it has been found that, without impurities, the magnetization oscillates periodically in a sawtooth pattern [22,23]. It is then expected that in silicene the magnetization also oscillates in a sawtooth pattern.

Because of the buckled nature of silicene, by applying a perpendicular electric field the spin and valley degeneracy of the LL is lifted [24]. In this case, in contrast with graphene, the energy levels of each valley are different and there is no more valley degeneracy. Moreover, considering the Zeeman effect, the LL for each spin split, loosing then the spin degeneracy. This loss of valley and spin degeneracy gives discontinuous changes in the last energy level, which in turn is expected to produce new magnetization peaks, as occur in graphene [25]. Motivated by this we have studied the

* Corresponding author at: Departamento de Física, Universidad Nacional del Sur, Av. Alem 1253, B8000CPB Bahía Blanca, Argentina.
E-mail addresses: federico.escudero@uns.edu.ar (F. Escudero), jsardenhi@gmail.com (J.S. Ardenghi), pvjasen@uns.edu.ar (P. Jasen).

https://doi.org/10.1016/j.jmmm.2018.01.060
0304-8853/

magnetic oscillations (MO) at $T = 0$ K in a general silicene-like system with a conduction electron density n_e, which could be due to an applied gate voltage.

We have organized the work as follow: In Section 2 we obtain the energy levels of silicene in a perpendicular magnetic and electric field, considering the intrinsic SOI and the Zeeman effect. From this we obtain an expression for the ground state internal energy and magnetization. In Section 3 we study and classify the MO peaks for different values of perpendicular electric field. In Section 4 we analyze the MO frequencies by performing a fast Fourier transform (FFT). Finally our conclusions follow in Section 5.

2. Magnetic oscillations in silicene

2.1. Energy spectrum

In the low wavelength approximation, with energies near the Fermi energy, the electrons in silicene are described by a Dirac-like Hamiltonian in 2D for massive fermions. In a perpendicular electric field E_z it reads [17]

$$H_{\eta s} = \upsilon_F(\eta\sigma_x p_x + \sigma_y p_y) + \sigma_z\Delta_{\eta s}, \tag{1}$$

where $\upsilon_F \sim 5.5\times10^5$ m/s is the Fermi velocity [18], σ_i are the Pauli matrices acting in the sublattices A and B, $\eta = 1\,(-1)$ for the valley K (K'), $s = \pm1$ for spin and down, and

$$\Delta_{\eta s} = \eta s\lambda_{SO} - elE_z, \tag{2}$$

where λ_{SO} is the intrinsic spin-orbit interaction (SOI) strength and l is the buckle height. We shall consider a perpendicular magnetic field B, so that $\mathbf{B} = B\mathbf{e}_z$. In the Landau gauge we have $\mathbf{A} = -By\mathbf{e}_x$, and the momentum changes following the Peierls substitution [26] $\mathbf{p}\to\mathbf{p} - e\mathbf{A}$. Considering the Zeeman effect [27], the term $\boldsymbol{\mu}\cdot\mathbf{B} = \mu_B g B s_z/2$ is added to H, where $s_z = 2S_z/\hbar$ is the Pauli matrix acting in the spin state. We omit the nearest- and next-nearest neighbor Rashba SOIs, denoted as λ_{R1} and λ_{R2} in [11], since they are negligible in comparison to the intrinsic SOI λ_{SO}. Then Eq. (1) becomes

$$H_{\eta s} = \upsilon_F\left[\eta\sigma_x(p_x + eBy) + \sigma_y p_y\right] + \sigma_z\Delta_{\eta s} - \boldsymbol{\mu}\cdot\mathbf{B}. \tag{3}$$

Because H only depends on the y coordinate, we can express the wave function as $\psi = e^{-ikx}\begin{pmatrix}\psi^A & \psi^B\end{pmatrix}$, with $\psi^{A/B}$ depending only on y. Then, introducing the ladder matrices $\sigma_\pm = \sigma_x \pm i\sigma_y$ and making the change of variable [28] $y' = (-\hbar k + eBy)/\sqrt{\hbar eB}$, the equation $H\psi = E\psi$ becomes

$$\left\{\upsilon_F\sqrt{\hbar eB}\left[\frac{\sigma_+}{2}(\eta y' - \partial_{y'}) + \frac{\sigma_-}{2}(\eta y' + \partial_{y'})\right] + \sigma_z\Delta_{\eta s} - \boldsymbol{\mu}\cdot\mathbf{B}\right\}\psi_{\eta s} = E\psi_{\eta s}. \tag{4}$$

Defining the ladder operators $a^\dagger = (y' - \partial_{y'})/\sqrt{2}$ and $a = (y' + \partial_{y'})/\sqrt{2}$ we get

$$\left[\eta\frac{\hbar\omega_L}{2}\left(\sigma_+\alpha_\eta^\dagger + \sigma_-\alpha_\eta\right) + \sigma_z\Delta_{\eta s} - \hbar\omega_Z s_z\right]\psi_{\eta s} = E\psi_{\eta s}, \tag{5}$$

where $\alpha_1 = a$, $\alpha_{-1} = a^\dagger$ and $\omega_L = \upsilon_F\sqrt{2eB/\hbar}$, $\omega_Z = \mu_B g B/2\hbar$. The energies can be calculated by writing the wave function for each valley and spin as

$$|\psi_s^\eta\rangle = b_s^\eta|n, A, s\rangle + c_s^\eta|n-\eta, B, s\rangle, \tag{6}$$

where b_s^η and c_s^η are constants, n is the Landau level (LL) index and $|s\rangle = |\pm\rangle$ represents the spin state, so that $s_z|s\rangle = s|s\rangle$. Then, given that $\sigma_+|A\rangle = 0, \sigma_+|B\rangle = 2|A\rangle, \sigma_-|A\rangle = 2|B\rangle$, $\sigma_-|B\rangle = 0$, $\sigma_z|A\rangle = |A\rangle$, $\sigma_z|B\rangle = -|B\rangle$ and $a^\dagger|n\rangle = \sqrt{n+1}|n+1\rangle, a|n\rangle = \sqrt{n}|n-1\rangle$, solving Eq. (5) the energy spectrum results

$$E_{0,\eta,s} = s\lambda_{SO} - \eta elE_z - s\hbar\omega_Z \quad (n = 0), \tag{7}$$

$$E_{n,\eta,s,\beta} = \beta\sqrt{(s\lambda_{SO} - \eta elE_z)^2 + (\hbar\omega_L)^2 n} - s\hbar\omega_Z \quad (n \geqslant 1), \tag{8}$$

where $\beta = -1$ for the valence band (VB) and $\beta = 1$ for the conduction band (CB). When $E_z = 0$, the LL have a doubly valley degeneracy, whereas when $E_z \neq 0$ this degeneracy vanishes. Notice that without the Zeeman effect the LL $n = 0$ is always twice less degenerate than the LL $n \geqslant 1$, regardless of E_z [24]. Therefore the Zeeman effect gives an equal degeneracy for all LL. Moreover, as in the classical case, each LL has a degeneracy due to the free direction (x in this case) which is not quantized. This degeneracy comes by imposing periodical boundary conditions and is given by $D = AB/\varphi$, where A is the silicene sheet area and $\varphi = h/e$ is the magnetic unit flux.

2.2. Ground state magnetization

We shall study the ground state magnetization ($T = 0$ K) for this system, under the influence of a perpendicular magnetic and electric field, where the energy levels are given by Eqs. (7) and (8). We consider a constant electron density $n_e = N/A$, which may due to an applied gate voltage, such that valence band is full and only the conduction band is available. The valence band would still make a continuous (non-oscillatory) contribution to the magnetization, but since we are interested only in the MO, we will not take this contribution into account. The internal energy at $T = 0$ K for the N conduction electrons can be computed as the sum of the filled Landau levels. The number of totally filled levels is $q = [q_c]$, where $q_c = N/D$ is the filling factor, and the brackets means the biggest integer less or equal to q_c (Floor function). It is worth noting that we assume that N is constant, instead of the the chemical potential μ (Fermi energy) being constant. However, for both cases the results are similar (see the Appendix for details).

In order to compute the ground state internal energy we have to sort the energy levels. We call ξ_m the decreasing sorted energy levels, $m = 0, 1, 2\ldots$ being the label index. In general we write[1]

$$\xi_m = \sqrt{(s_m\lambda_{SO} - \eta_m elE_z)^2 + (\hbar\omega_L)^2 n_m} - s_m\hbar\omega_Z, \tag{9}$$

where $s_m = \pm1$ gives the spin, $n_m = 0, 1, 2\ldots$ the LL and $\eta_m = \pm1$ the valley for the m position. If we denote $\theta = q_c - q = N/D - [N/D]$ to the occupancy factor of the last unfilled Landau level, the internal energy at $T = 0$ K is

$$U = \sum_{m=0}^{q-1} D\xi_m + D\theta\xi_q. \tag{10}$$

In Eq. (9) we separate $\xi_m = \xi_m^0 - s_m\hbar\omega_Z$, with $\xi_m^0 = \sqrt{(s_m\lambda_{SO} - \eta_m elE_z)^2 + (\hbar\omega_L)^2 n_m}$. Replacing in Eq. (10) we can write

$$U = U_0 - D\hbar\omega_Z\left[\sum_{m=0}^{q-1} s_m + \theta s_q\right], \tag{11}$$

where

$$U_0 = \sum_{m=0}^{q-1} D\xi_m^0 + D\theta\xi_q^0. \tag{12}$$

The last term in Eq. (11) can be related to the Pauli paramagnetism associated with the spin population. This can be seen by considering N_+ and N_- total number of spin up and down, respectively. For q levels filled, let k_+ be the number of (+1) values and k_- the number of (-1) values in the sorting function s_m, with $m = 0, 1, \ldots, q-1$ (thus k_+ and k_- represents the number of spin up and down states

[1] For the LL $n = 0$ only the positive root should be taken. See Eq. (7).

totally filled, respectively). Consequently, $k_+ + k_- = q$ and $\sum_{m=0}^{q-1} s_m = k_+ - k_-$. For the last unfilled level there could be two cases: (i) it is spin up or (ii) spin down. For spin up, $s_q = 1$ and therefore we can write the total number of spin up and down as $N_+ = Dk_+ + D\theta s_q$ and $N_- = Dk_-$. Thus using that $\sum_{m=0}^{q-1} s_m = k_+ - k_-$ we have $N_+ - N_- = D\left[\sum_{m=0}^{q-1} s_m + \theta s_q\right]$. The same result holds if the last unfilled level is spin down. Therefore the Pauli magnetization is

$$M_P = \mu_B(N_+ - N_-) = \mu_B D\left[\sum_{m=0}^{q-1} s_m + \theta s_q\right]. \tag{13}$$

Notice that this result is independent of how the energy levels are sorted, so that the last term in Eq. (11) is always related to the Pauli paramagnetism. Consequently, because $\hbar\omega_Z = \mu_B B$, Eq. (11) becomes

$$U = U_0 - BM_P. \tag{14}$$

The magnetization at $T = 0$ K is $M = -\partial U/\partial B$. From Eq. (14) we have

$$M = M_0 + M_P + B\frac{\partial M_P}{\partial B}, \tag{15}$$

where $M_0 = -\partial U_0/\partial B$. Given that $\partial D/\partial B = D/B$, $\partial\theta/\partial B = -N/(DB)$ and $\partial\xi_m^0/\partial B = (\hbar\omega_L)^2 n_m/2B\xi_m^0 = \left[\xi_m^0 - (s_m\lambda_{SO} - \eta_m elE_z)^2/\xi_m^0\right]/2B$, we have

$$M_0 = \frac{1}{B}\left(N\xi_q^0 - \frac{3}{2}U_0\right) + M', \tag{16}$$

where

$$M' = \frac{D}{2B}\left[\sum_{m=0}^{q-1}\frac{(s_m\lambda_{SO} - \eta_m elE_z)^2}{\xi_m^0} + \theta\frac{\left(s_q\lambda_{SO} - \eta_q elE_z\right)^2}{\xi_q^0}\right]. \tag{17}$$

This new contribution M' to the magnetization is not present in graphene [25] due to the negligible SOI and zero buckle height. On the other hand, from Eq. (13) we get $\partial M_P/\partial B = M_P/B + \mu_B D s_q \partial\theta/\partial B = (M_P - \mu_B N s_q)/B$. Therefore, from Eqs. (9), (14) and (16), the total ground state magnetization given by Eq. (15) can be written as

$$M = \frac{1}{B}\left(N\xi_q - \frac{3}{2}U\right) + M' + \frac{1}{2}M_P. \tag{18}$$

This is the fundamental equation for our analysis. It shows that the MO peaks are produced whenever ξ_q, M' or M_P changes discontinuously, U being continuous always. Thus the magnetization in pristine silicene at $T = 0$ K oscillates in a sawtooth pattern, as in graphene [23,25] and in general 2DEG with a Dirac-like spectrum [22]. This is also in agreement with the results found in [29], where the MO at $T = 0$ K in a pristine buckled honeycomb lattice are expressed as an infinite sum of harmonics k of the form $\sin(k)/k$, which gives a sawtooth oscillation. From Eq. (18) we write the MO peak amplitude ΔM as

$$\Delta M = \frac{N}{B}\Delta\xi_q + \Delta M' + \frac{1}{2}\Delta M_P. \tag{19}$$

The first contribution $\Delta\xi_q$ comes directly from the discontinuous change in the last energy level, which occurs only when the filling factor q changes. On the other hand, by analyzing Eqs. (13) and (17) we see that the MO peaks produced by $\Delta M'$ and/or ΔM_P occur when the parameters η_q and s_q change but ξ_q remains continuous. This would happen if the change in η_q and s_q does not come from a change in the filling factor q.

Eq. (18) also allows an intuitive interpretation of the effect that impurities have in the magnetization. In the pristine case, the discontinuities in ξ_q, M' or M_P are essentially a product of the discrete LL, which gives a delta-like density of states (DOS) and causes the MO to be sawtooth-like. But when impurities are added to the system, the DOS is broaden and the discontinuities in ξ_q, M' or M_P disappear. Consequently, the MO are also broaden and the oscillations are no more sawtooth like.

2.3. LL, valley and spin mixing

We are interested in how the parameters n_q, η_q and s_q vary with B for different values of elE_z. We recall that n_q may takes values $0, 1, 2, \ldots$, while $\eta_m = 1\,(-1)$ for the $K\,(K')$ valley and $s_m = 1\,(-1)$ for spin up (down). The value of these parameters depends on the sorted position q, which in turn depends in the mixing of the LL, valley and spin. We consider a conduction electron density $n_e = 0.01\ \text{nm}^{-2}$ and an area $A = 1000\ \text{nm}^2$. In Fig. 1 we show the parameters n_q, η_q and s_q as a function of B for different values of elE_z.

In Fig. 1(a) we can see the case $E_z = 0$, where there is no parameter η_q because each energy level in Eq. (9) has a doubly valley degeneracy. The last energy level ξ_q changes discontinuously only whenever the LL n_q, the spin s_q or both change. When $E_z \neq 0$, the valley degeneracy is broken and the energy levels start to depend on η_q. This can be seen in Fig. 1(b), where for $elE_z = 5$ meV the parameters start to vary differently. Nevertheless, it should be noted that in both Fig. 1(a) and (b) there is no appreciable mixing of the parameters. This means that in each case n_q is always decreasing (as B is increased), while η_q and s_q always alternate in the same way between -1 and 1. Moreover, in either case both M' and M_p are always continuous because every change in the parameters is produced by a change in the filling factor q, so $\Delta M' = 0 = \Delta M_p$ in Eq. (19). As E_z increases, the parameters start to vary in a more complicated way. This can be seen in Fig. 1(c), in the case $elE_z = 64$ meV, where there is a notorious mixing of the parameters, which implies that M' and M_p may not be always continuous. In such case all three contributions in Eq. (19) will be present.

3. Classification of MO peaks

We showed in Eq. (18) that the MO peaks are produced by the discontinuous changes in ξ_q, M' or M_P, which in turn depends on n_q, η_q and s_q. This allows a classification of the MO peaks according to the parameters that change. We can define seven general types of peaks, considering the change of LL, valley or spin and its combinations. This can be seen in Table 1.

Furthermore, each type of MO peak has its own subpeaks, corresponding to different possible ways in which the parameters can change. The type of subpeak can be identified from the change in n_q, η_q and s_q. In general we label the subpeaks as $X^{\bar{n}}_{\bar{\eta},\bar{s}}$, where $X = \{L, LV, LS, LVS, V, VS, S\}$ identifies the type of MO peaks, as classify in Table 1, and $\bar{n}$, $\bar{\eta}$ and $\bar{s}$ indicate the change (or not) of the parameters. For example, consider an LS peak corresponding to a change of LL $n = 5 \to 4$ and spin $\uparrow\to\downarrow$, in the valley K. Then we identify this peak with $LS^{5\to4}_{K,\uparrow\to\downarrow}$.

The defined classification of MO peaks provides a systematic way of recognizing them in a magnetization graph. One procedure could be to first analyze how the energy levels are sorted (as done in Section 2.3), from which one could predict which type of MO

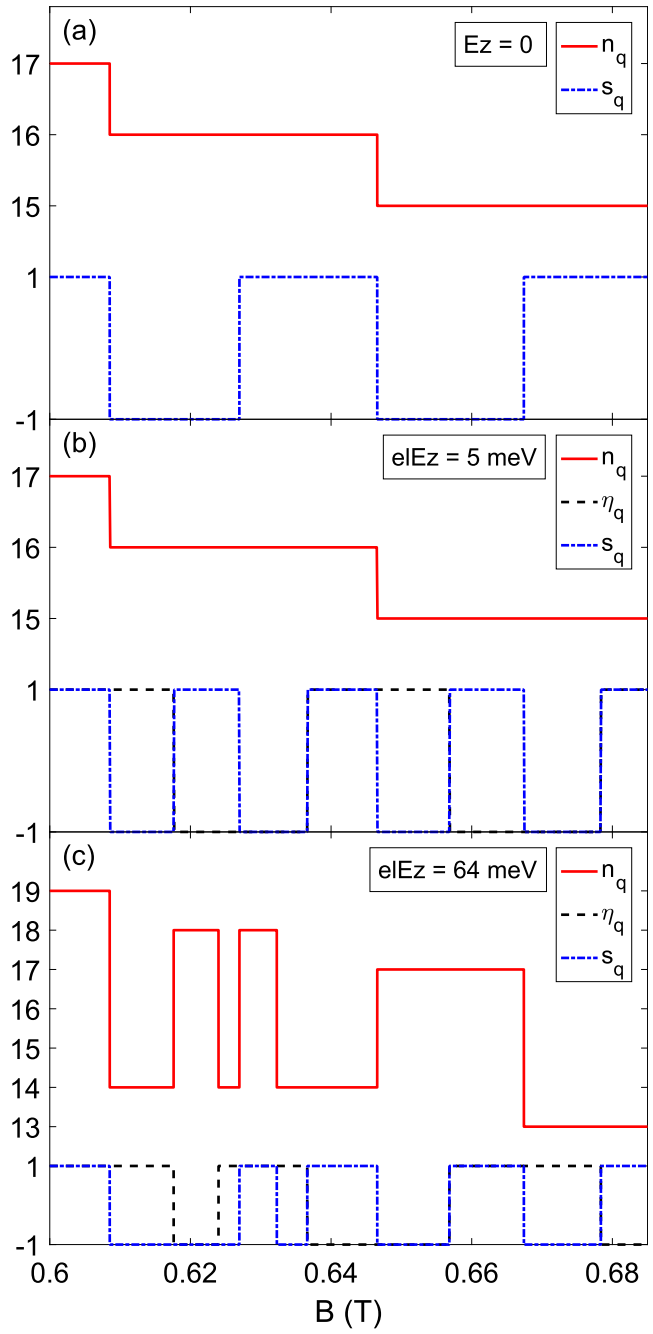

Fig. 1. Parameters n_q (LL), η_q (valley) and s_q (spin) as a function of the magnetic field B, for (a) $E_z = 0$, (b) $elE_z = 5$ meV and (c) $elE_z = 64$ meV.

Table 1
Classification of MO peaks according to the change in the parameters n_q (LL), η_q (valley) and s_q (spin).

LL change	Valley change	Spin change	Type of MO peak
✓	×	×	L
✓	✓	×	LV
✓	×	✓	LS
✓	✓	✓	LVS
×	✓	×	V
×	✓	✓	VS
×	×	✓	S

peak appear and in which order. We shall do this first for the case $elE_z \ll 1$ eV, and then for the general case in which elE_z may take any value. In all cases we shall take $0.6 < B[T] < 0.685$, as in Fig. 1.

3.1. Limit $elE_z \ll 1$ eV

We consider low elE_z such that the parameters change only when the filling factor q does it. Hence in this regime both M' and M_p are continuous and only $\Delta\xi_q$ contributes to the MO peaks in Eq. (19). We will consider the cases $E_z = 0$ and $elE_z = 5$ meV, when the sorting of the parameters is given by Fig. 1. Then, following the classification of Table 1, we see in Fig. 1(a) that the possible type of MO peaks at $E_z = 0$ are LS and S, with the order LS, S, LS, S,...On the other hand, we see in Fig. 1(b) that at $elE_z = 5$ meV the MO peaks are LS, VS and S, with the order LS, VS, S, VS, LS...These results can be seen in Fig. 2, where we plot the magnetization (18) for $E_z = 0$ and $elE_z = 5$ meV.

For $E_z = 0$ we effectively see that only the peaks LS and S appear. The S peaks always correspond to a change of spin down to up, so its amplitude is always $\Delta M_s = 2N\mu_B$ at $E_z = 0$. When $elE_z = 5$ meV, the VS peak appears, and the order of the peaks is LS, VS, S, VS, S,..., as expected. The LS peak always correspond to a change of spin up to down in a K valley. The VS peak corresponds to $\{K \to K', \downarrow \to \uparrow\}$ or $\{K' \to K, \downarrow \to \uparrow\}$, while the S peak always correspond to a change of spin up to down in the K' valley. Thus, from Eqs. (9) and (19) we can write the corresponding peaks amplitude

$$\Delta M_{LS} = \frac{N}{B}\left[\chi(n_q; -elE_z) - \chi(n_q - 1; +elE_z)\right] - 2N\mu_B, \tag{20}$$

$$\Delta M_{VS} = 2N\mu_B, \tag{21}$$

$$\Delta M_S = \frac{N}{B}\left[\chi(n_q; +elE_z) - \chi(n_q; -elE_z)\right] - 2N\mu_B, \tag{22}$$

where $\chi(n_q; \pm elE_z) = \sqrt{(\lambda_{SO} \pm elE_z)^2 + (\hbar\omega_L)^2 n_q}$, with n_q being the corresponding LL level, as indicated in Fig. 2. The VS peak always has the same amplitude $2N\mu_B$, which is equal to ΔM_s in the case $E_z = 0$. In the limit $elE_z \ll 1$ we can approximate the subpeaks amplitude in Eqs. (20) and (22) by

$$\frac{B}{N}\Delta M_{LS} \simeq \varrho_+ - 2\hbar\omega_Z - \lambda_{SO} elE_z \varrho_-, \tag{23}$$

$$\frac{B}{N}\Delta M_S \simeq \left[\gamma_q^{-1}(\lambda_{SO}, \omega_L) 2\lambda_{SO}\right] elE_z - 2\hbar\omega_Z, \tag{24}$$

where $\varrho_\pm = \gamma_q^{\pm 1}(\lambda_{SO}, \omega_L) \mp \gamma_{q-1}^{\pm 1}(\lambda_{SO}, \omega_L)$, with $\gamma_q(\lambda_{SO}, \omega_L) \equiv \sqrt{\lambda_{SO}^2 + (\hbar\omega_L)^2 n_q}$.

Thus the peaks amplitude is linear with E_z, with both the slope and the y-intercept depending on λ_{SO} and ω_L. By studying how the amplitude of the peaks vary with E_z, one could obtain the parameters λ_{SO} and ω_L, provided that the magnetic field B and n_q of the peaks are known. It is important to notice that for each peak the magnetic field B and n_q are different. The Landau level n_q could be inferred knowing at which B the type of peak occur, and how is the sorting of the energy levels. For instance, when $elE_z = 5$ meV, we know that the sorting is given by Fig. 1(b). Thus, the second peak LS in Fig. 2(b) corresponds to a change of LL from $n = 16 \to 15$, so we put $n_q = 16$ in Eq. (23).

This way of obtaining λ_{SO} and ω_L from the MO peaks could be an useful alternative to the other available methods. The Landau energy ω_L gives the Fermi velocity, since we define $\omega_L = v_F\sqrt{2eB/\hbar}$. In silicene, the Fermi velocity has usually been obtained using DFT or TB models, with the result of a lower value than in graphene [4,6,18]. This can be easily understood from the reduced hopping in silicene since the Si atoms are more distant from each other. Likewise, the SO parameter λ_{SO} is usually obtained from TB models using the hopping parameters [7].

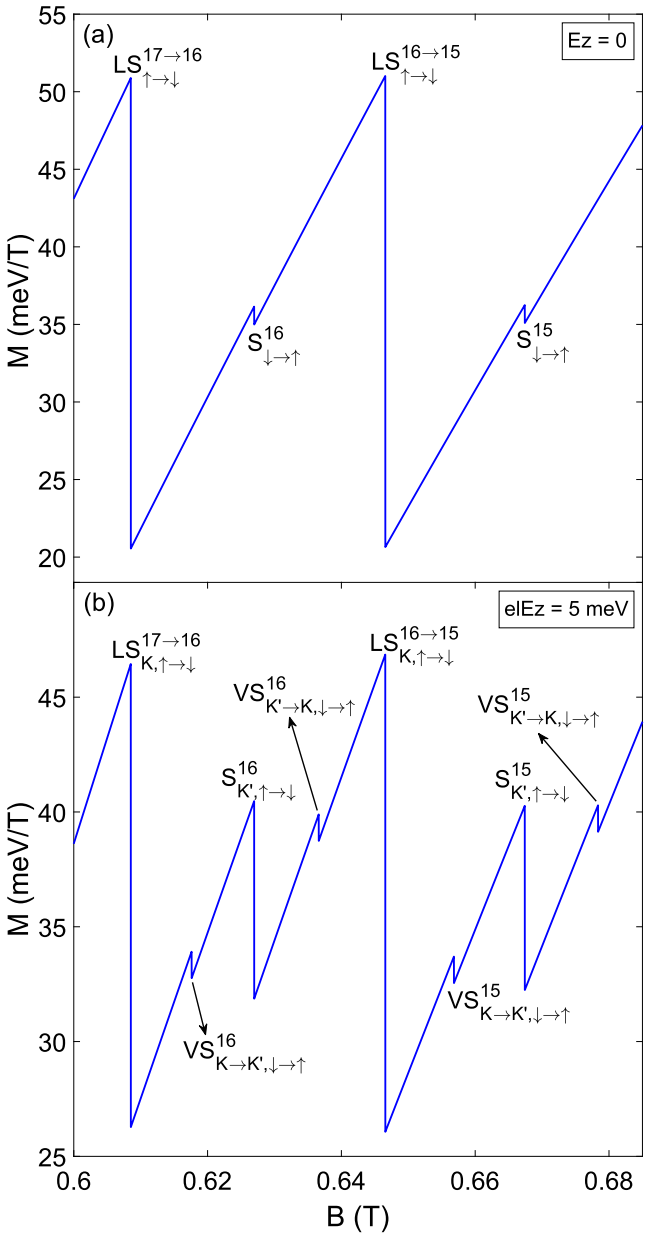

Fig. 2. Magnetization given by Eq. (18) for (a) $E_z = 0$ and (b) $elE_z = 5$ meV.

3.2. General case

In the general case the mixing of the parameters n_q, η_q and s_q depends on the specific value of elE_z. We saw in Fig. 1(c) that these parameters vary in a complicated way as elE_z increases. Thus for any specific value of electric field one should see how the energy levels are sorted in order to identify the MO peaks. Moreover, in the general case M' and M_P may no longer be continuous, and the contributions $\Delta M'$ and ΔM_p should be taken into account in Eq. (19).

We consider $elE_z = 64$ meV, in which case n_q, η_q and s_q as a function of B are given in Fig. 1(c). Then we can identify ten MO peaks for $0.6 < B[T] < 0.685$. For instance, the first is a LS peak corresponding to $\{K, \uparrow\to\downarrow\}$, while the sixth is a VS peak corresponding to $\{K \to K', \downarrow\to\uparrow\}$.

In the same way one can classify the other peaks, leading to the magnetization for $elE_z = 64$ meV shown in Fig. 3.

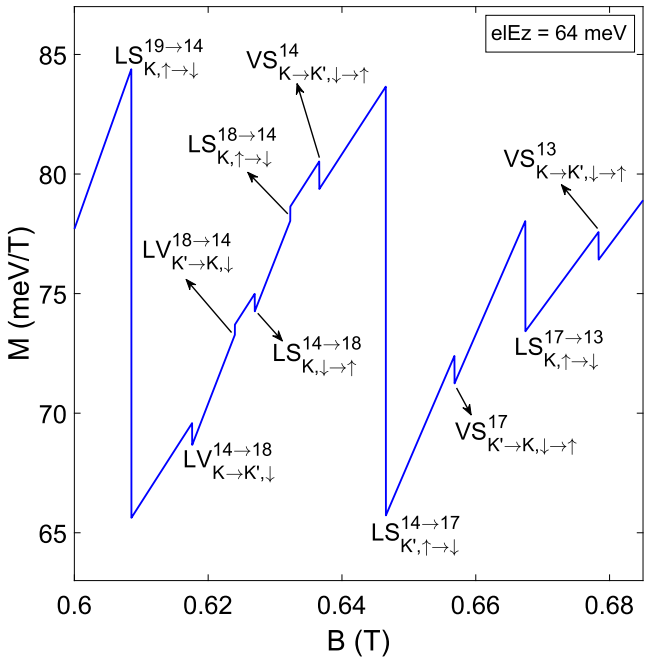

Fig. 3. Magnetization given by Eq. (18) for $elE_z = 64$ meV.

As we see, the mixing of the parameters alters drastically the magnetization. In particular we note that in the two peaks $LV^{18\to14}_{K'\to K,\downarrow}$ and $LS^{18\to14}_{K,\uparrow\to\downarrow}$ the magnetization increases, which is opposite to all other peaks, where the magnetization always decreases. This feature suggests that the peaks $LV^{18\to14}_{K'\to K,\downarrow}$ and $LS^{18\to14}_{K,\uparrow\to\downarrow}$ are not produced by the change $\Delta\xi_q$, but come from the discontinuities in M' and M_p. Indeed, the contribution $\Delta\xi_q$ always lower the magnetization because it comes from the discontinuous change in the last energy level ξ_q as B increases. To see this we plot in Fig. 4 the variation of ξ_q, M' and M_P with respect to B, for $elE_z = 64$ meV.

We can clearly appreciate two discontinuities in M' and one discontinuity in M_P. We also see that when this discontinuities occur ξ_q is continuous,[2] which implies $\Delta\xi_q = 0$. Thus the peaks $LV^{18\to14}_{K'\to K,\downarrow}$ and $LS^{18\to14}_{K,\uparrow\to\downarrow}$ are effectively produced by $\Delta M'$ and ΔM_p. The first peak $LV^{18\to14}_{K'\to K,\downarrow}$ only has contribution from $\Delta M'$ because only the valley changes. This can be seen in Fig. 4, where when the first discontinuity occurs in M' we see that M_P is continuous. On the other hand, the peak $LS^{18\to14}_{K,\uparrow\to\downarrow}$ has both contributions $\Delta M'$ and ΔM_p, as can be seen in Fig. 4, where both M' and M_P have a discontinuity. In this way we can say, in general, that the MO peaks that increase the magnetization are not produced by the discontinuous change in the last energy level ξ_q, but rather by the discontinuous change in M' and/or M_P.

4. MO frequencies

So far we have analyzed only the MO peaks amplitude, but we can also obtain information from their frequencies. For simplicity we shall consider the cases $E_z = 0$ and $elE_z = 5$ meV, such that the only contribution in Eq. (19) is given by $\Delta\xi_q$ and all the MO peaks can occur only when the filling factor q changes. Given that $q = [N/D] = [n_e\varphi/B]$, it is clear that the magnetization oscillates periodically as a function of $1/B$, in agreement with the Onsager

[2] Nevertheless we can see that the slope of ξ_q slightly changes when M' or M_P are discontinuous. The reason for this is that the variation of the parameters in this places do modify ξ_q, but in a continuous way, giving a different dependence with B without any discontinuous jump.

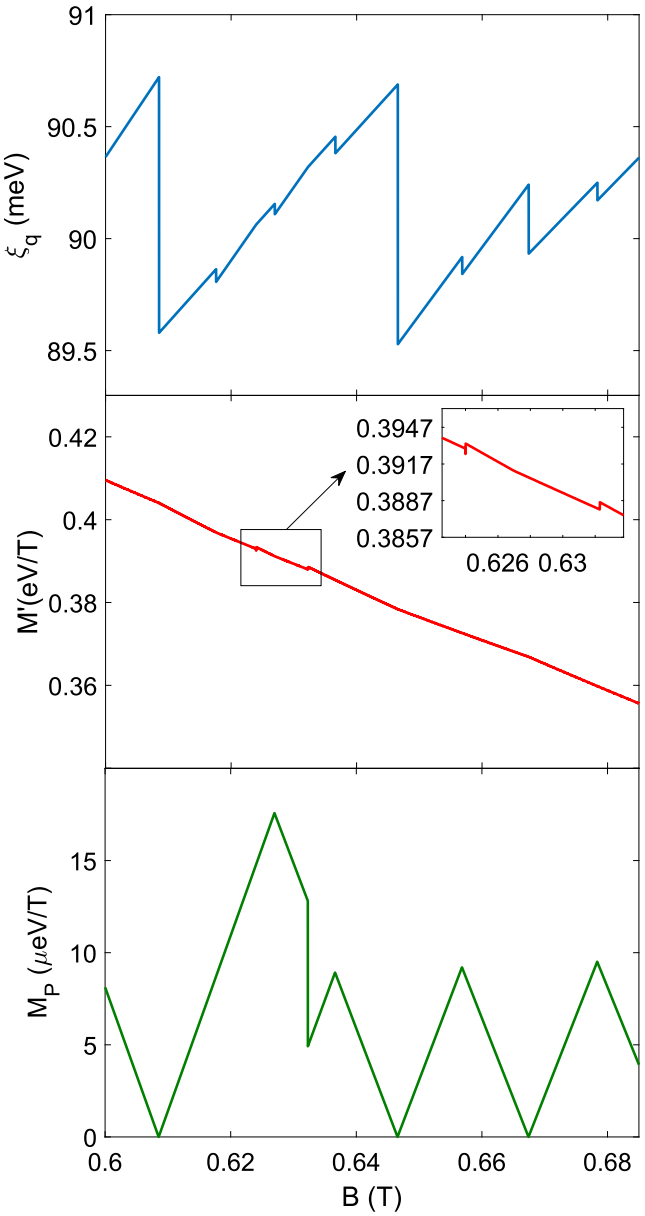

Fig. 4. ξ_q, M' and M_P given by Eqs. (9), (13) and (17), as a function of B, in the case $elE_z = 64$ meV.

relation [21]. The period of oscillation is in general given by $\Delta(1/B) = 1/B_2 - 1/B_1$, where $B_1 = n_e\varphi/q_1$ and $B_2 = n_e\varphi/q_2$ ($\varphi = h/e$). Thus we can write

$$\Delta\left(\frac{1}{B}\right) = \frac{e}{2\pi\hbar n_e}\Delta q, \tag{25}$$

where $\Delta q = q_2 - q_1$. Because the MO are sawtooth like, there will be many frequencies involved in its Fourier expansion. Nevertheless we are interested only in the fundamental frequencies, for the others are just harmonics of these ones. To obtain the frequency spectrum we performed a fast Fourier transform (FFT) in the magnetization as a function of $1/B$.

In Fig. 5 we can appreciate the case $E_z = 0$, where the MO are a combination of two sawtooth oscillations (SO) with different frequencies, as can be inferred in the FFT spectrum, where two main frequencies $\omega_1 = 10.33$ T and $\omega_2 = 20.7$ T can be recognized. This can be explained if we decompose the term ξ_q in Eq. (18), which causes the SO with its discontinuous change. When $E_z = 0$ we have,

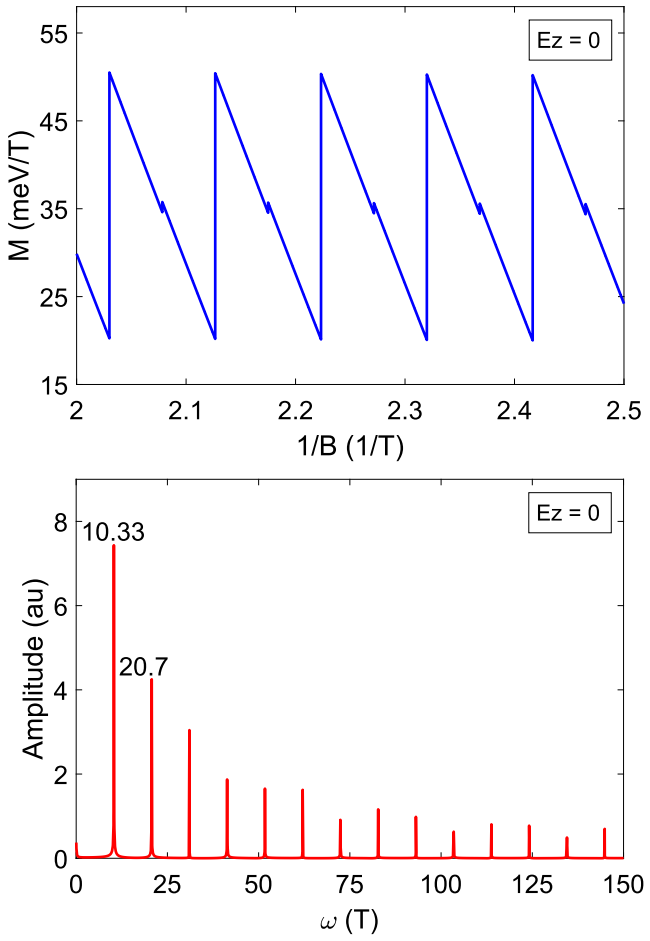

Fig. 5. Magnetization and fast Fourier transform (FFT) for $E_z = 0$.

from Eq. (9), $\xi_q = \sqrt{\lambda_{SO}^2 + (\hbar\omega_L)^2 n_q} - s_q\hbar\omega_Z = \xi_q^L - \xi_q^S$, where we separated

$$\xi_q^L = \sqrt{\lambda_{SO}^2 + (\hbar\omega_L)^2 n_q}, \tag{26}$$

$$\xi_q^S = s_q\hbar\omega_Z. \tag{27}$$

The term ξ_q^L is only related to the LL, while the term ξ_q^S is only related to the spin. Then, considering the parameters sorting given by Fig. 1(a), and taking into account the valley degeneracy at $E_z = 0$, we get that ξ_q^L changes periodically when q changes by four, so $\Delta q = 4$ in Eq. (25), giving the frequency $\omega_1 = \pi\hbar n_e/2e$. On the other hand, ξ_q^S changes periodically when q changes by two, so $\Delta q = 2$ in Eq. (25), giving the frequency $\omega_2 = \pi\hbar n_e/e$. Thus the magnetization in Eq. (18) can be decomposed in two SO with two different fundamental frequencies. For the considered electron density $n_e = 0.01$ nm^{-2} we obtain $\omega_1 = 10.34$ T and $\omega_2 = 20.68$ T, in agreement with Fig. 5.

When $elE_z = 5$ meV the valley degeneracy is broken, which gives rise to another MO frequency $\omega_3 = 41.37$ T, as seen in Fig. 6. The origin of this can be explained by first approximating ξ_q for low elE_z, so $\xi_q \simeq \sqrt{\lambda_{SO}^2 + (\hbar\omega_L)^2 n_q} - s_q\hbar\omega_Z - elE_z\lambda_{SO}s_q\eta_q \left[\lambda_{SO}^2 + (\hbar\omega_L)^2 n_q\right]^{-1/2}$. This can be separated as $\xi_q = \xi_q^L - \xi_q^S - \xi_q^{VS}$, where ξ_q^L and ξ_q^S are given by Eqs. (26) and (27), while

$$\xi_q^{VS} = elE_z \frac{\lambda_{SO}\eta_q s_q}{\sqrt{\lambda_{SO}^2 + (\hbar\omega_L)^2 n_q}}. \tag{28}$$

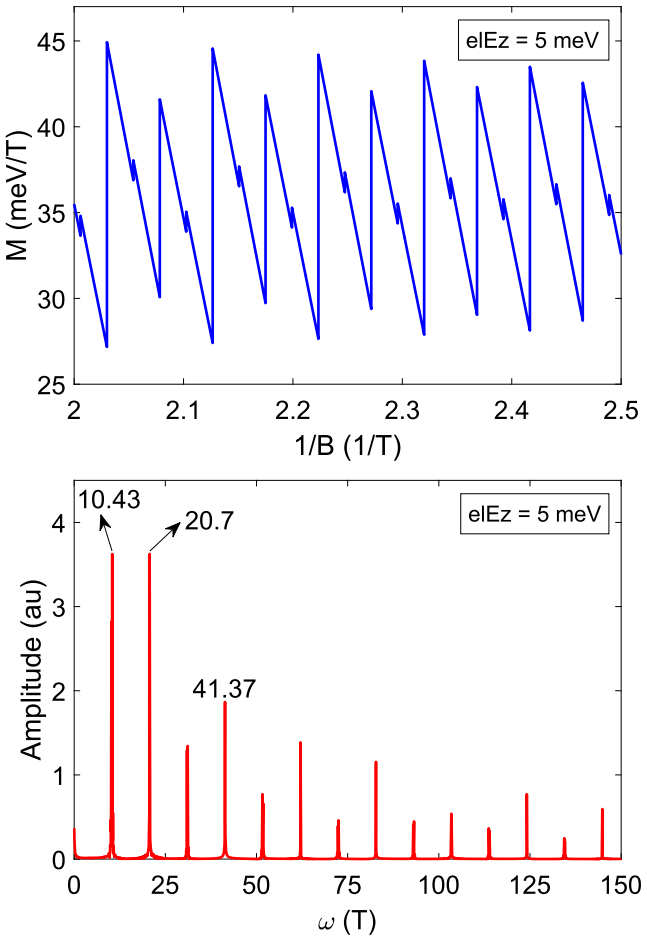

Fig. 6. Magnetization and fast Fourier transform (FFT) for $elE_z = 5$ meV.

For $elE_z = 5$ meV, the sorting of the parameters n_q, η_q and s_q is given by Fig. 1(b). Hence n_q still changes only q changes by four, so ξ_q^L gives the frequency $\omega_1 = \pi\hbar n_e/2e = 10.34$ T. On the other hand, now s_q changes whenever q changes, so for ξ_q^S we have $\Delta q = 1$ in Eq. (25). This gives a new frequency $\omega_3 = 2\pi\hbar n_e/e$ which implies $\omega_3 = 41.36$ T for $n_e = 0.01$ nm^{-2}. Finally, the new defined term ξ_q^{VS} in Eq. (28) changes discontinuously when $\Delta q = 2$, as can be easily seen in Fig. 1(b). Therefore we also have the frequency $\omega_2 = \pi\hbar n_e/e = 20.68$ T.

5. Conclusions

We studied the magnetic oscillations (MO) in pristine silicene at $T = 0$ K. We considered a constant electron density, such that the valence band is full and only the conduction band is available. Under a perpendicular electric and magnetic field, we found analytical expressions for the ground state internal energy and magnetization. We obtained that the MO are sawtooth-like and are entirely produced by the change in the last energy level occupied. This lead us to a classification of the MO peaks in terms of the parameters n_q (LL), η_q (valley) and s_q (spin) which define the last energy level. In general we defined seven types of MO peaks, as indicated in Table 1. Using this classification we analyzed the MO in the case of low electric field ($elE_z \ll 1$ eV), and the general case in which E_z may take any value. In each case we were able to classify the type of MO present, and in which order. When $E_z = 0$ the energy levels have a valley degeneracy and the MO peaks occur only when the last occupied level changes its LL and/or spin. On the other hand, when $E_z \neq 0$ the valley degeneracy is broken and new MO peaks appear, associated with the change of valley in the last energy level. Furthermore, we found that analyzing the MO peak amplitude one could extract information about the Fermi velocity and the spin–orbit interaction strength, which could be an useful alternative to the other available methods. For the general case of E_z the last energy level varies in a complicated way and therefore so does it the MO peaks. Nevertheless one can still classify the peaks by studying the change in the parameters n_q, η_q and s_q at any particular E_z. Finally we analyzed the MO frequencies, where we found that the magnetization effectively oscillates periodically a function of $1/B$. We performed the fast Fourier transform spectrum of the sawtooth-like MO oscillations. When $E_z = 0$ we found two fundamental frequencies, corresponding to the change of LL or spin in the last energy level. When $elE_z = 5$ meV a new fundamental frequency appears, associated with the broken valley degeneracy.

Acknowledgment

This paper was partially supported by grants of CONICET (Argentina National Research Council) and Universidad Nacional del Sur (UNS) and by ANPCyT through PICT 2014-1351. Res. N270/15. N: 2014-1351, and PIP 2014-2016. Res. N5013/14. Cdigo: 11220130100436CO research grant, as well as by SGCyT-UNS., J.S. A. and P.J. are members of CONICET., F.E. acknowledge research fellowship from this institution.

Appendix A. Magnetization for constant Fermi energy

We shall analyze the case in which the Fermi energy μ is held constant, instead of the conduction electron density n_e. We consider $\mu > 0$ such that last energy level filled always correspond to the CB. The valence band is not taken into account since it is full and thus will not contribute to the MO. Because we consider μ fixed, whereas the number of electrons N may change, we work with the grand potential Ω. For a Fermi energy μ, all energies levels $m = 0, 1, 2 \ldots, m_F$ all filled, where m_F is such that $\xi_{m_F} \leqslant \mu \leqslant \xi_{m_{F+1}}$. Then the grand potential Ω at $T = 0$ K is

$$\Omega = \sum_{m=0}^{m_F} D(\xi_m - \mu), \tag{A.1}$$

where ξ_m is given by Eq. (9). Separating $\xi_m = \xi_m^0 - s_m\hbar\omega_Z$, with $\xi_m^0 = \sqrt{(s_m\lambda_{SO} - \eta_m elE_z)^2 + (\hbar\omega_L)^2 n_m}$, we get

$$\Omega = \Omega_0 - D\hbar\omega_Z \sum_{m=0}^{q-1} s_m, \tag{A.2}$$

where

$$\Omega_0 = \sum_{m=0}^{m_F} D(\xi_m^0 - \mu). \tag{A.3}$$

As in the case with N constant, the last term in Eq. (A.2) is related to the Pauli paramagnetism associated with the spin population, with the difference that this time all the energy levels below the Fermi energy are completely filled. Thus the Pauli paramagnetism is $M_P = \mu_B(N_+ - N_-) = \mu_B D\sum_{m=0}^{m_F} s_m$, and Eq. (A.2) becomes

$$\Omega = \Omega_0 - BM_P. \tag{A.4}$$

This result is similar to the one obtained in Eq. (14), with U being replaced by Ω. Therefore, similar expressions are obtained for the magnetization, given by $M = -(\partial\Omega/\partial B)_\mu$. From Eq. (A.4) we obtain

$$M = -\frac{1}{2B}(3\Omega + N\mu) + M' + \frac{1}{2}M_P, \tag{A.5}$$

where $N = \sum_{m=0}^{m_F} D = D(m_F - 1)$ is the number of electrons, and

$$M' = \frac{D}{2B}\sum_{m=0}^{m_F} \frac{(s_m\lambda_{SO} - \eta_m elE_z)^2}{\xi_m^0}. \tag{A.6}$$

Eq. (A.5) shows that, when μ is constant, the MO peaks are produced whenever N, M' or M_P changes discontinuously, with Ω being continuous always. Then in general we write the MO peak amplitude ΔM as

$$\Delta M = -\frac{\mu}{2B}\Delta N + \Delta M' + \frac{1}{2}\Delta M_P. \tag{A.7}$$

This last equation is similar to Eq. (19), with each contribution ΔN, $\Delta M'$ and ΔM_P being still defined by the discontinuous change in the parameters n_q, η_q and s_q. The main difference is that in this case, with μ constant, all the three functions N, M' and M_P have discontinuities at any E_z. Nevertheless, one could still classify the MO peaks as done in Table 1, which accounts for the main results found in the case when N is constant.

References

[1] A. Kara, H. Enriquez, A.P. Seitsonen, L.L.Y. Voon, S. Vizzini, B. Aufray, H. Oughaddou, A review on silicene – new candidate for electronics, Surf. Sci. Rep. 67 (1) (2012) 1–18, https://doi.org/10.1016/j.surfrep.2011.10.001.

[2] M. Houssa, A. Dimoulas, A. Molle, Silicene: a review of recent experimental and theoretical investigations, J. Phys.: Condens. Matter 27 (25) (2015) 253002, https://doi.org/10.1088/0953-8984/27/25/253002.

[3] J. Zhuang, X. Xu, H. Feng, Z. Li, X. Wang, Y. Du, Honeycomb silicon: a review of silicene, Sci. Bull. 60 (18) (2015) 1551–1562, https://doi.org/10.1007/s11434-015-0880-2.

[4] G.G. Guzmán-Verri, L.C.L.Y. Voon, Electronic structure of silicon-based nanostructures, Phys. Rev. B 76 (7) (2007), https://doi.org/10.1103/physrevb.76.075131, 075131.

[5] M. Houssa, E. Scalise, K. Sankaran, G. Pourtois, V.V. Afanas'ev, A. Stesmans, Electronic properties of hydrogenated silicene and germanene, Appl. Phys. Lett. 98 (22) (2011) 223107, https://doi.org/10.1063/1.3595682.

[6] S. Cahangirov, M. Topsakal, E. Aktürk, H. Şahin, S. Ciraci, Two- and one-dimensional honeycomb structures of silicon and germanium, Phys. Rev. Lett. 102 (23) (2009) 23680, https://doi.org/10.1103/physrevlett.102.236804.

[7] C.-C. Liu, H. Jiang, Y. Yao, Low-energy effective hamiltonian involving spin-orbit coupling in silicene and two-dimensional germanium and tin, Phys. Rev. B 84 (19) (2011) 195430, https://doi.org/10.1103/PhysRevB.84.195430.

[8] Y. Yao, F. Ye, X.-L. Qi, S.-C. Zhang, Z. Fang, Spin-orbit gap of graphene: first-principles calculations, Phys. Rev. B 75 (4) (2007), https://doi.org/10.1103/physrevb.75.041401, 041401.

[9] C.-C. Liu, W. Feng, Y. Yao, Quantum spin hall effect in silicene and two-dimensional germanium, Phys. Rev. Lett. 107 (7) (2011), https://doi.org/10.1103/PhysRevLett. 107.076802, 076802.

[10] X.-T. An, Y.-Y. Zhang, J.-J. Liu, S.-S. Li, Quantum spin hall effect induced by electric field in silicene, Appl. Phys. Lett. 102 (4) (2013), https://doi.org/10.1063/1.4790147, 043113.

[11] M. Ezawa, Quantum hall effects in silicene, J. Phys. Soc. Jpn. 81 (6) (2012), https://doi.org/10.1143/JPSJ.81.064705, 064705.

[12] M. Ezawa, Spin valleytronics in silicene: quantum spin hall-quantum anomalous hall insulators and single-valley semimetals, Phys. Rev. B 87 (15) (2013) 155415, https://doi.org/10.1103/physrevb.87.155415.

[13] N.D. Drummond, V. Zlyomi, V.I. Fal'ko, Electrically tunable band gap in silicene, Phys. Rev. B 85 (7) (2012) 3702, https://doi.org/10.1103/PhysRevB.85.075423.

[14] Z. Ni, Q. Liu, K. Tang, J. Zheng, J. Zhou, R. Qin, Z. Gao, D. Yu, J. Lu, Tunable bandgap in silicene and germanene, Nano Lett. 12 (1) (2012) 113–118, https://doi.org/10.1021/nl203065e.

[15] Y. Liu, X. Zhou, M. Zhou, M.-Q. Long, G. Zhou, Electric field induced spin and valley polarization within a magnetically confined silicene channel, J. Appl. Phys. 116 (24) (2014) 244312, https://doi.org/10.1063/1.4904751.

[16] V. Vargiamidis, P. Vasilopoulos, G.-Q. Hai, Dc and ac transport in silicene, J. Phys.: Condens. Matter 26 (34) (2014) 345303, https://doi.org/10.1088/0953-8984/26/34/345303.

[17] M.J. Spencer, T. Morishita (Eds.), Silicene, Springer International Publishing, 2016, https://doi.org/10.1007/978-3-319-28344-9.

[18] N.Y. Dzade, K.O. Obodo, S.K. Adjokatse, A.C. Ashu, E. Amankwah, C.D. Atiso, A.A. Bello, E. Igumbor, S.B. Nzabarinda, J.T. Obodo, A.O. Ogbuu, O.E. Femi, J.O. Udeigwe, U.V. Waghmare, Silicene and transition metal based materials: prediction of a two-dimensional piezomagnet, J. Phys.: Condens. Matter 22 (37) (2010) 375502, https://doi.org/10.1088/0953-8984/22/37/375502.

[19] C.J. Tabert, E.J. Nicol, Valley-spin polarization in the magneto-optical response of silicene and other similar 2d crystals, Phys. Rev. Lett. 110 (19) (2013) 197402, https://doi.org/10.1103/PhysRevLett. 110.197402.

[20] D. Shoenberg, The de haas-van alphen effect, Philos. Trans. R. Soc. A: Math. Phys. Eng. Sci. 245 (891) (1952) 1–57, https://doi.org/10.1098/rsta.1952.0016.

[21] L. Onsager, Interpretation of the de haas-van alphen effect, The London, Edinburgh, Dublin Philos. Mag. J. Sci. 43 (344) (1952) 1006–1008, https://doi.org/10.1080/14786440908521019.

[22] S.G. Sharapov, V.P. Gusynin, H. Beck, Magnetic oscillations in planar systems with the dirac-like spectrum of quasiparticle excitations, Phys. Rev. B 69 (7) (2004) 125124, https://doi.org/10.1103/PhysRevB.69.075104.

[23] S. Zhang, N. Ma, E. Zhang, The modulation of the de haas–van alphen effect in graphene by electric field, J. Phys.: Condens. Matter 22 (11) (2010) 115302, https://doi.org/10.1088/0953-8984/22/11/115302.

[24] K. Shakouri, P. Vasilopoulos, V. Vargiamidis, F.M. Peeters, Integer and half-integer quantum hall effect in silicene: Influence of an external electric field and impurities, Phys. Rev. B 90 (23) (2014) 235423, https://doi.org/10.1103/PhysRevB.90.235423.

[25] F. Escudero, J. Ardenghi, L. Sourrouille, P. Jasen, Ground state magnetization of conduction electrons in graphene with zeeman effect, J. Magn. Magn. Mater. 429 (2017) 294–298, https://doi.org/10.1016/j.jmmm.2016.12.032.

[26] R. Peierls, Zur theorie des diamagnetismus von leitungselektronen, Zeitschrift für Physik 80 (11–12) (1933) 763–791, https://doi.org/10.1007/BF01342591.

[27] P. Zeeman, VII.doublets and triplets in the spectrum produced by external magnetic forces, Philos. Mag. Ser. 5 44 (266) (1897) 55–60, https://doi.org/10.1080/14786449708621028.

[28] J. Ardenghi, P. Bechthold, P. Jasen, E. Gonzalez, O. Nagel, Landau level transitions in doped graphene in a time dependent magnetic field, Physica B 427 (2013) 97–105, https://doi.org/10.1016/j.physb.2013.06.037.

[29] C.J. Tabert, J.P. Carbotte, E.J. Nicol, Magnetic properties of dirac fermions in a buckled honeycomb lattice, Phys. Rev. B 91 (3) (2015), https://doi.org/10.1103/PhysRevB.91.035423, 035423.